JACS
JOURNAL OF THE AMERICAN CHEMICAL SOCIETY

Article

pubs.acs.org/JACS

A Combined Mössbauer, Magnetic Circular Dichroism, and Density Functional Theory Approach for Iron Cross-Coupling Catalysis: Electronic Structure, In Situ Formation, and Reactivity of Iron-Mesityl-Bisphosphines

Stephanie L. Daifuku,[†] Malik H. Al-Afyouni,[†] Benjamin E. R. Snyder, Jared L. Kneebone, and Michael L. Neidig*

Department of Chemistry, University of Rochester, Rochester, New York 14627, United States

Supporting Information

ABSTRACT: While iron-bisphosphines have emerged as effective catalysts for C−C cross-coupling, the nature of the in situ formed iron species, elucidation of the active catalysts and the mechanisms of catalysis have remained elusive. A combination of ^{57}Fe Mössbauer and magnetic circular dichroism (MCD) spectroscopies of well-defined and in situ formed mesityl-iron(II)-SciOPP species combined with density functional theory (DFT) investigations provides the first direct insight into electronic structure, bonding and in situ speciation of mesityl-iron(II)-bisphosphines in the Kumada cross-coupling of MesMgBr and primary alkyl halides using $FeCl_2$(SciOPP). Combined with freeze-trapped solution Mössbauer studies of reactions with primary alkyl halides, these studies demonstrate that distorted square-planar $FeMes_2$(SciOPP) is the active catalyst for cross-coupling and provide insight into the molecular-level mechanism of catalysis. These studies also define the effects of key reaction protocol details, including the role of the slow Grignard addition method and the addition of excess SciOPP ligand, in leading to high product yields and selectivities.

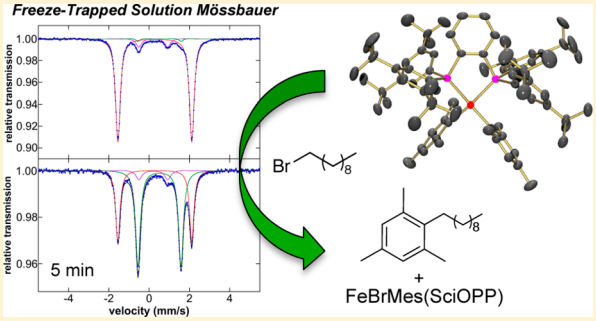

1. INTRODUCTION

Iron-catalyzed C−C cross-coupling reactions have attracted significant interest as more cost-effective and sustainable alternatives to traditional precious metal catalysts. Importantly, iron catalysts have demonstrated high activity and selectivity in cross-coupling reactions that have proven difficult for precious metal catalysts, such as the coupling of unactivated alkyl halides with Grignard reagents.[1−4] Since the initial reports of these reactions with simple iron salts by Kochi in the 1970s,[5−7] research over the past decade has led to the successful development of several new iron-based C−C cross-coupling reaction systems, including those employing bisamine (e.g., TMEDA),[8−11] NHC[12−16] and bisphosphine (e.g., SciOPP,[17−19] dpbz,[20,21] dppe[22]) ligands.

Iron-bisphosphines have emerged as particularly attractive systems for a variety of C−C cross-coupling reactions, including those with organozinc (Negishi), aryl Grignards (Kumada), alkynyl Grignards (Sonogoshira-type) and organoboron (Suzuki−Miyaura) nucleophiles. For example, $FeCl_2(dpbz)_2$ is a highly effective precatalyst for Negishi-type cross-coupling reactions of aryl zinc reagents and alkyl electrophiles.[20,23] Bedford and co-workers have also shown that dppe can be an effective bisphosphine ligand for the Negishi-type cross-coupling reactions catalyzed with dppbz ligand,[24] further expanding the scope and utility of iron-bisphosphine precatalysts. Nakamura and Chai have also demonstrated that Xantphos is an effective ligand that facilitates selective alkyl−alkyl cross-coupling with iron.[25,26] The $FeCl_2$(SciOPP) precatalyst developed by Nakamura and co-workers (Scheme 1) is an especially versatile precatalyst for cross-coupling due to its utility in Kumada,[18] Suzuki−Miyaura,[17,27] Negishi[21,28,29] and Sonogashira-type[19] cross-couplings in high yield and good selectivity for heterocoupling over homocoupling, including the efficient Kumada cross-coupling of bulky MesMgBr with primary alkyl halides[18] (Scheme 2) and benzyl halides.[30]

Despite the success of iron-catalyzed cross-coupling reactions including those with iron-bisphosphines, the design and development of improved catalysts requires a detailed understanding of in situ formed iron species and mechanism of catalysis in these systems. Numerous challenges exist in studying iron cross-coupling systems that have historically hindered their investigation relative to other systems such as those with palladium. For example, the prevalence of paramagnetism in iron species involved in cross-coupling as well as the need to elucidate the individual iron species present in potentially complex mixtures are two major obstacles. Furthermore, characterization methods that can evaluate both the geometric and electronic structures of the in situ formed

Received: April 10, 2014
Published: May 29, 2014

   dx.doi.org/10.1021/ja503596m | J. Am. Chem. Soc. 2014, 136, 9132−9143

Scheme 1. $FeCl_2$(SciOPP) Catalyzed C−C Cross-Couplings

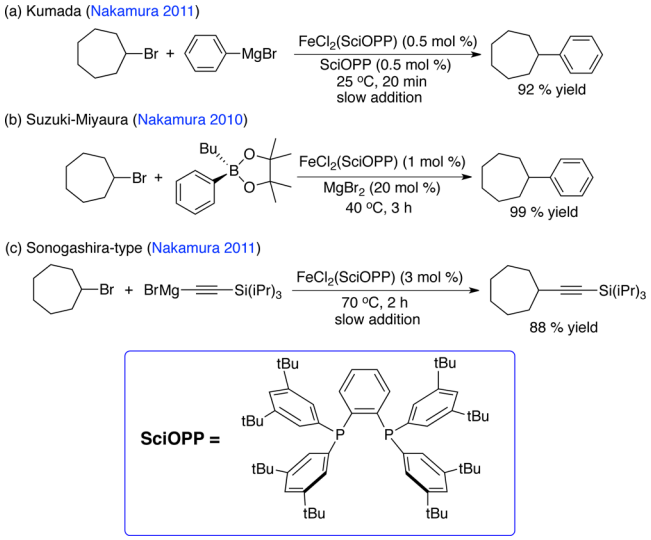

Scheme 2. $FeCl_2$(SciOPP) Catalyzed Kumada Cross-Coupling of MesMgBr and Primary Alkyl Halides[18]

iron species (including those present as minor components) would provide the greatest insight into the origins of reactivity in iron cross-coupling systems. To understand reactivity and identify active catalytic species, it is essential to directly determine the reactivity of iron species formed in situ. Key reactivity studies include the determination of which individual iron species in complex mixtures react with electrophiles, the kinetics of their reactions and the iron species formed following reaction. Combined with traditional gas chromatography (GC) studies of product formation, such investigations would provide direct insight into the mechanism of catalysis.

The application of an experimental methodology combining ^{57}Fe Mössbauer and magnetic circular dichroism (MCD) spectroscopies of freeze-trapped solutions with inorganic synthesis, catalytic reaction studies, and density functional theory (DFT) investigations offers a powerful approach to address these challenges and define the active species and mechanisms involved in iron-catalyzed cross-coupling. In the present study, the utility of this approach is demonstrated in the study of the Kumada cross-coupling of MesMgBr and primary alkyl halides (Scheme 2). Electronic structure and bonding are evaluated in mesityl-iron(II)-SciOPP complexes using a combination of ^{57}Fe Mössbauer, MCD and DFT/TD-DFT methods: FeBrMes(SciOPP) and $FeMes_2$(SciOPP). Furthermore, the direct elucidation of the mesitylated iron(II) species formed in situ from reaction of $FeCl_2$(SciOPP) with MesMgBr are determined and quantified. Direct evaluation of the in situ reactions with primary alkyl halides in single-turnover and catalytic reactions is also reported using Mössbauer and MCD spectroscopies coupled to GC studies, where time-resolved, freeze-trapped Mössbauer spectroscopy permits the quantitative determination of the pseudo-first-order rates of reaction with 1-bromodecane. These investigations provide direct insight into the active species and mechanism of catalysis present in the Kumada cross-coupling of primary alkyl halides with MesMgBr by $FeCl_2$(SciOPP).

2. RESULTS AND ANALYSIS

2.1. Synthesis, Spectroscopic Characterization, and Electronic Structure Calculations of $FeMes_2$(SciOPP) and FeBrMes(SciOPP). In order to study electronic structure, bonding and reactivity in mesitylated iron-SciOPP complexes, $FeMes_2$(SciOPP) and FeBrMes(SciOPP) were prepared. The reaction of 2.2 equiv of MesMgBr with $FeCl_2$(SciOPP) in THF

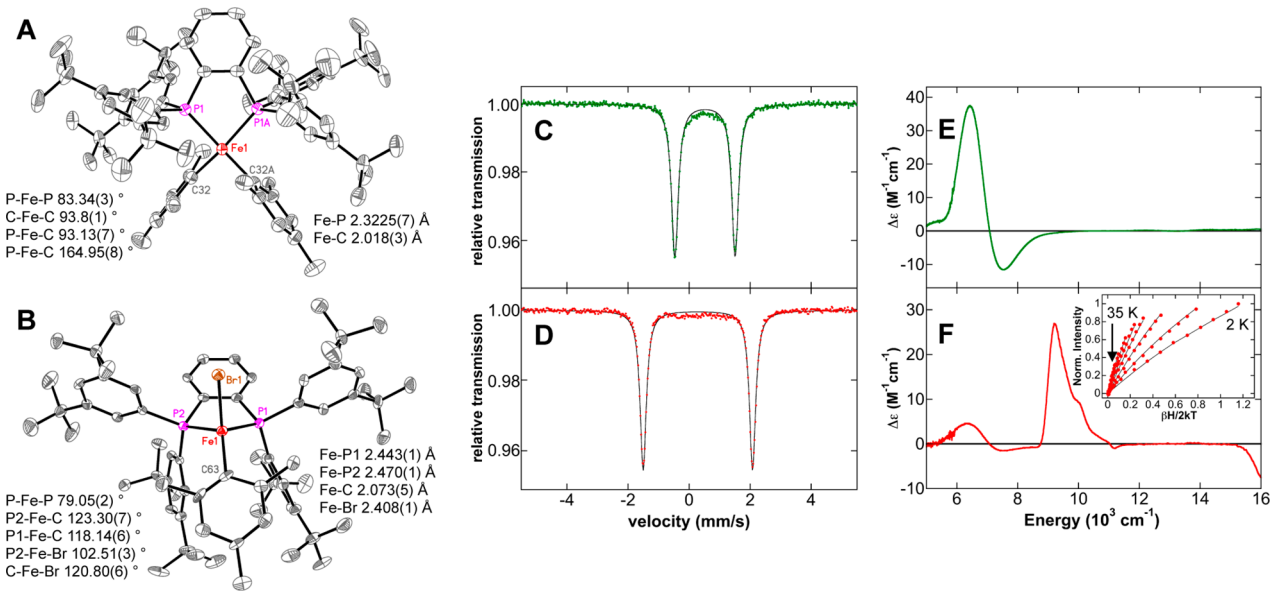

Figure 1. X-ray, Mössbauer, and MCD characterization of mesityl-iron(II)-SciOPP complexes X-ray crystal structures of (A) $FeMes_2$(SciOPP) and (B) FeMesBr(SciOPP). Select bond distances and angles are given for each structure, and thermal ellipsoids are shown at the 50% probability level. 80 K Mössbauer spectrum of solid (C) FeBrMes(SciOPP) and (D) $FeMes_2$(SciOPP). 5 K, 7 T NIR MCD spectrum of (E) FeBrMes(SciOPP) and (F) $FeMes_2$(SciOPP). (F, inset) VTVH-MCD data (dots) and fit (lines) of $FeMes_2$(SciOPP) collected at 10 000 cm^{-1}.

dx.doi.org/10.1021/ja503596m | J. Am. Chem. Soc. 2014, 136, 9132−9143

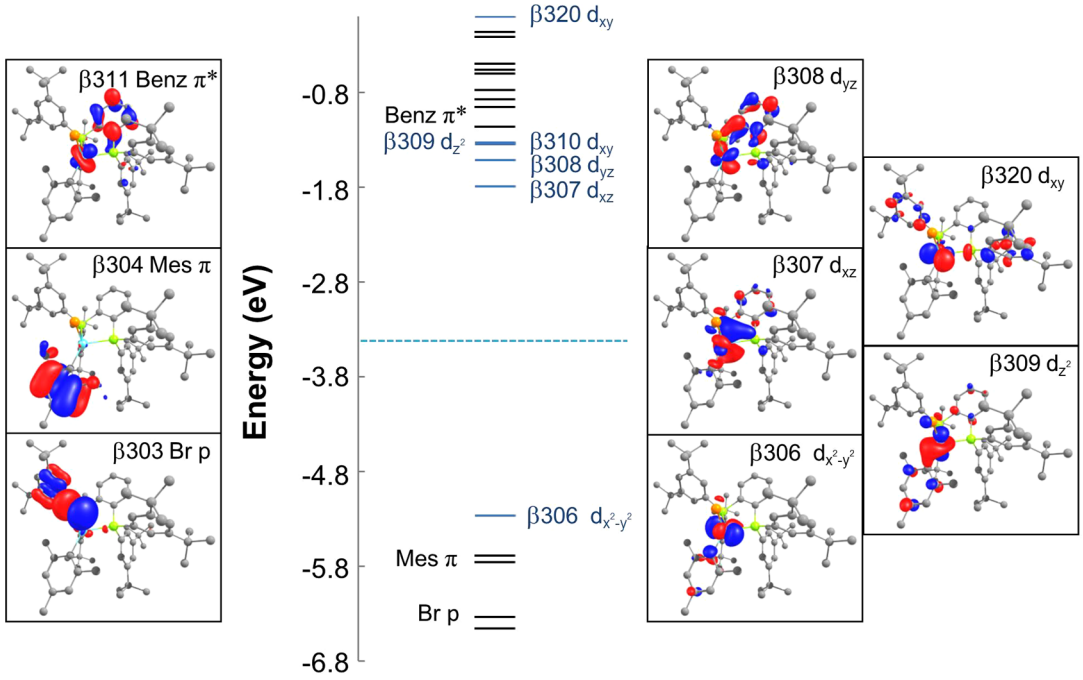

Figure 2. Calculated molecular orbital energy diagram for FeBrMes(SciOPP).

at −30 °C was found to produce $FeMes_2$(SciOPP) as confirmed by X-ray crystallography (Figure 1A). The solid-state structure of $FeMes_2$(SciOPP) is best described as a distorted square-planar complex with Fe−P bond distances (2.32 Å) dramatically reduced compared to those previously reported for $FeCl_2$(SciOPP) (Fe−P 2.44/2.46 Å).[17] The synthesis of $FeMes_2$(SciOPP) from the reaction of Fe_2Mes_4 with SciOPP has also recently been demonstrated by Fürstner and co-workers, though no X-ray crystal structure was reported.[31] The corresponding monomesitylated FeBrMes(SciOPP) complexes could also be synthesized from an analogous method in the reaction of 1 equiv of MesMgBr with $FeBr_2$(SciOPP) in THF at room temperature. X-ray crystallography (Figure 1B) confirmed the formation of FeBrMes(SciOPP), which is best described in the solid-state structure as a distorted tetrahedron.

The 80 K ^{57}Fe Mössbauer spectrum of solid FeBrMes(SciOPP) (Figure 1C) is well described by a single iron species with δ = 0.52 mm/s and ΔE_Q = 1.97 mm/s. The 5 K, 7 T NIR MCD spectrum of FeBrMes(SciOPP) (Figure 1E) contains two low energy LF transitions at 6460 and 7460 cm^{-1} (10Dq(T_d) ∼ 6960 cm^{-1}, Δ^5T_2 ∼ 1000 cm^{-1}), consistent with the distorted tetrahedral geometry of the high-spin S = 2 complex. FeBrMes(SciOPP) exhibits an effective magnetic moment in C_6D_6 (Evans method) consistent with its description as a high-spin S = 2 iron(II) species (μ_{eff} = 5.0(3) μ_B). The 80 K Mössbauer spectrum of FeClMes(SciOPP) (see Supporting Information (SI), Figure S2) has similar Mössbauer parameters (δ = 0.53 mm/s and ΔE_Q = 1.87 mm/s) to FeBrMes(SciOPP). FeClMes(SciOPP) exhibits an effective magnetic moment in C_6D_6 (Evans method) consistent with its description as a high-spin S = 2 iron(II) species (μ_{eff} = 4.9(3) μ_B). The 298 K UV−vis absorption and 5 K, 7 T UV−vis MCD spectra of FeBrMes(SciOPP) contain multiple high energy charge transfer (CT) transitions, which are assigned using TD-DFT calculations and discussed in detail in the SI.

The 80 K ^{57}Fe Mössbauer of solid $FeMes_2$(SciOPP) (Figure 1D) is well described by a single iron species with δ = 0.29 mm/s and ΔE_Q = 3.58 mm/s. This isomer shift is consistent with those previously reported for square-planar iron-phosphine complexes with bis(mesityl) ligation (e.g., $FeMes_2$(dppe): δ = 0.33 mm/s and ΔE_Q = 4.53 mm/s),[32] while the reduction in the quadrapole splitting is consistent with the distortion away from pure square-planar geometry in $FeMes_2$(SciOPP). The NIR MCD spectrum of this complex (Figure 1F) in solution exhibits three LF transitions at ∼6350, 7530, and 9300 cm^{-1} in addition to a negative tail at <16 000 cm^{-1}, which corresponds to the lowest energy CT transition observed in the UV−vis MCD at 16 890 cm^{-1} (see SI). There are also numerous additional CT bands in the UV−vis region which are evaluated and discussed in the SI using TD-DFT. Saturation magnetization data collected at 10 000 cm^{-1} (Figure 1F, inset) is well described by a S = 1 ground state with ground-state spin-Hamiltoniam parameters of g_{iso} ∼2.1 cm^{-1}, with D = 1191 ± 2 cm^{-1} and E/D = 0.1.[33] The effective magnetic moment of $FeMes_2$(SciOPP) was determined in solution by the Evans method in C_6D_6 (μ_{eff} = 4.1(3) μ_B). The large shift of the observed μ_{eff} value from the spin-only value for S = 1 (μ_{eff}^{SO} = 2.8 μ_B), slightly larger than previously reported μ_{eff} values for square-planar S = 1 mesityl-iron(II)-phosphines,[32] is likely due to second order spin−orbit coupling and/or unquenched orbital angular momentum in $FeMes_2$(SciOPP).

Spin unrestricted DFT calculations were used to further probe the electronic structures of FeBrMes(SciOPP) and $FeMes_2$(SciOPP). Geometry optimization with PBEPBE/TZVP yielded overall structural features, bond lengths and angles in good agreement to those observed by crystallography.[34] As a general trend, slightly longer metal−ligand bonds were observed in the calculated structures (in solvent), consistent with slight bond elongation in solution. Evaluations of molecular orbitals, energies and transition energies were subsequently calculated from the optimized structures using B3LYP/TZVP in a tetrahydrofuran PCM model.

dx.doi.org/10.1021/ja503596m | J. Am. Chem. Soc. 2014, 136, 9132−9143

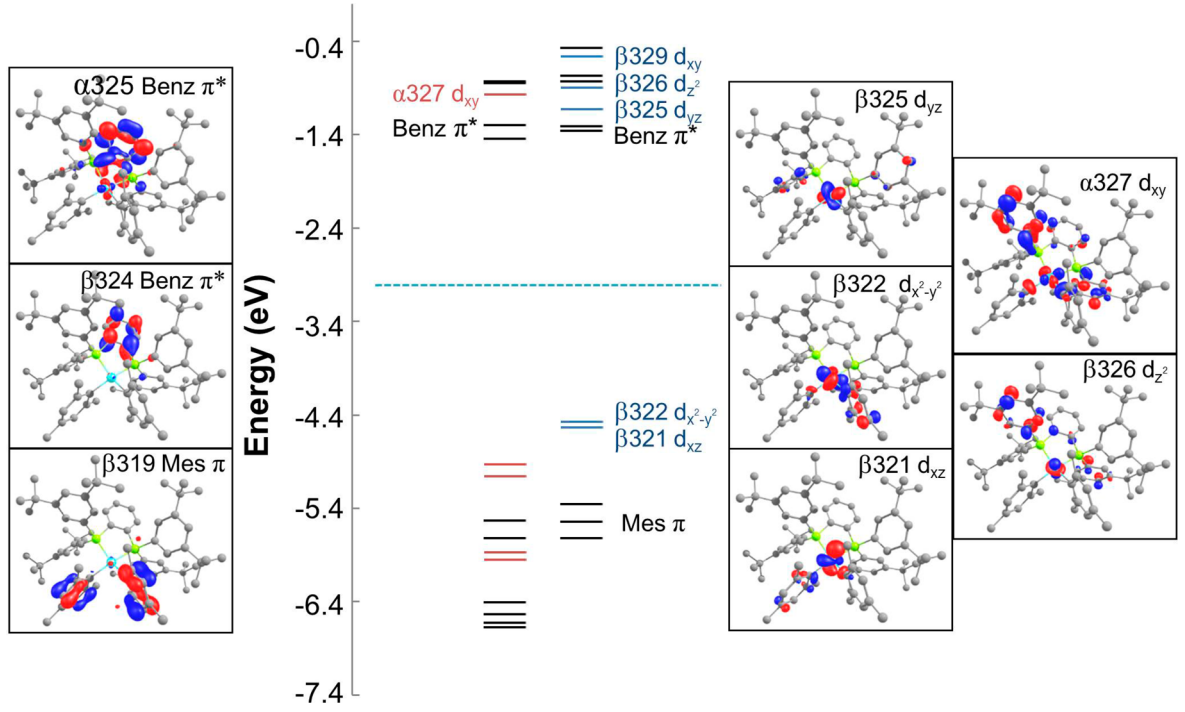

Figure 3. Calculated molecular orbital energy diagram for $FeMes_2$(SciOPP).

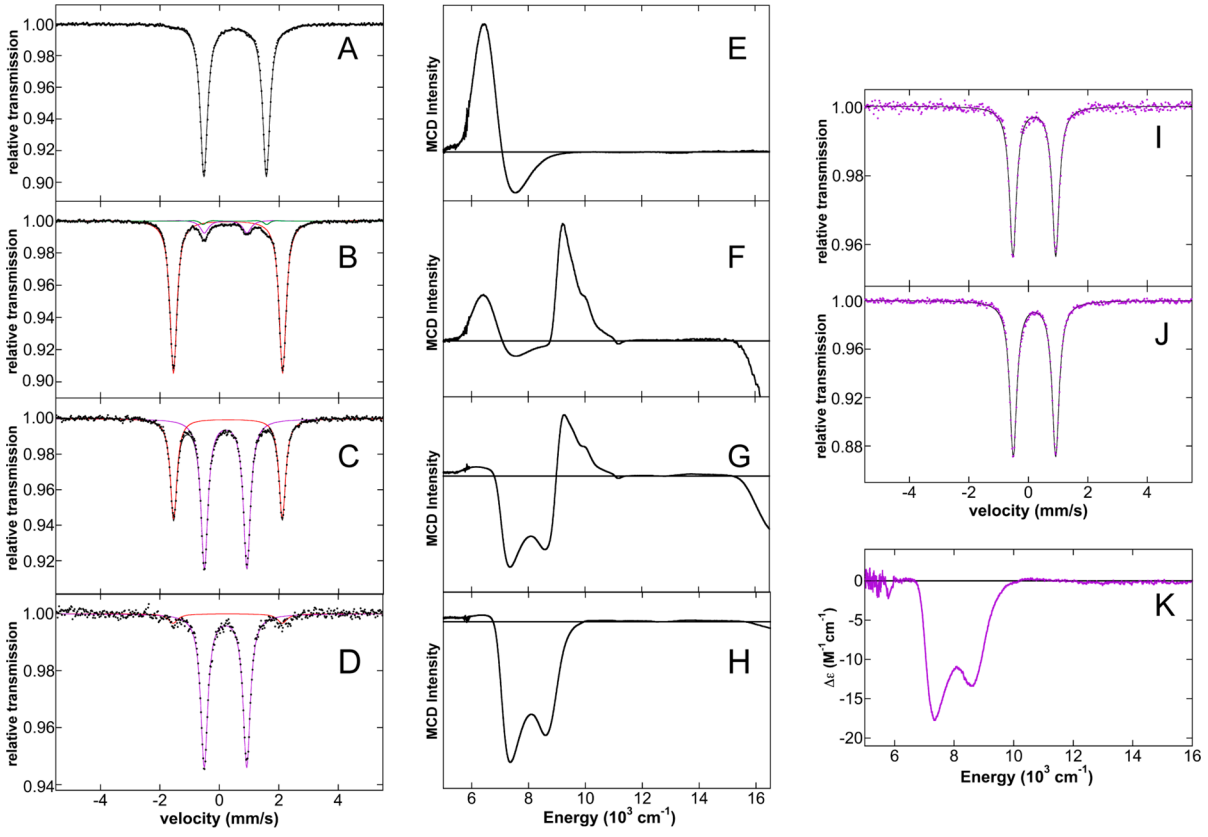

Figure 4. ^{57}Fe Mössbauer and NIR MCD spectroscopy of in situ formed iron species in reactions of $^{57}FeCl_2$(SciOPP) with MesMgBr. (A–D) 80 K ^{57}Fe Mössbauer spectra from reaction of $FeCl_2$(SciOPP) (3 mM) with (A) 1 equiv, (B) 2 equiv, (C) 20 equiv and (D) 100 equiv of MesMgBr. Data (black dots) and total fit (black lines) are shown. Individual component fits are shown and described in the text. (E–H) 5 K, 7 T NIR MCD spectra from reaction of $FeCl_2$(SciOPP) (3 mM) with (E) 1 equiv, (F) 2 equiv, (G) 20 equiv and (H) 100 equiv of MesMgBr. (I) 80 K ^{57}Fe Mössbauer spectrum of solid $FeMes_3^-$. (J) 80 K ^{57}Fe Mössbauer spectrum of in situ generated $FeMes_3^-$ from reaction of $^{57}FeCl_2$·1.5THF (3 mM) with 3 equiv of MesMgBr. (G) 5 K, 7 T NIR MCD spectrum of $FeMes_3^-$ (3 mM). All solution samples were prepared in 1:1 THF:2-MeTHF. Mössbauer fit analysis errors are $\delta \pm 0.02$ mm/s, $\Delta E_Q \pm 2\%$ and percentage of total iron ± 3%.

dx.doi.org/10.1021/ja503596m | J. Am. Chem. Soc. 2014, 136, 9132–9143

The optimized FeBrMes(SciOPP) complex is a distorted tetrahedron with Fe−P bonds of 2.44 and 2.43 Å, Fe−Br bond of 2.43 Å, Fe−C bond of 2.03 Å, and P−Fe−C bond angles of 125.8° and 125.1°. This optimized geometry is in good agreement with the crystal structure, which has Fe−P bonds of 2.44 and 2.47 Å, Fe−Br bond of 2.41 Å, Fe−C bond of 2.07 Å and P−Fe−C bond angle of 118.1°. Experimental and computational studies of FeBrMes(SciOPP) complex are consistent with a high-spin iron(II) complex (S = 2). The ground state wave function of this complex is characterized by the frontier molecular orbitals (FMOs), which represent two occupied MOs of mesityl (Mes) π character followed by one occupied and four unoccupied β Fe d MOs mixed with phosphorus p character (Figure 2). Because of significant covalency in the structure, significant d_{xy} contributions can be found in the β310 and β320 MOs, with 41 and 43% d character, respectively. Predominant Fe−P bonding of the FMOs is described by π-bonding of phosphorus p orbitals with the d_{xz} and d_{yz} orbitals (β307 and β308, respectively). Unoccupied benzene backbone (Benz) π^* interactions participate in π-bonding through phosphorus p orbitals to Fe as seen in β308.

The optimized $FeMes_2$(SciOPP) complex is a distorted square-plane with Fe−P bonds of 2.32 Å, Fe−C bonds of 2.01 Å and P−Fe−C bond angles of 93.7°. This $FeMes_2$(SciOPP) optimized geometry is in good agreement to the crystal structure which has Fe−P bonds of 2.32 Å, Fe−C bonds of 2.02 Å, and P−Fe−C bond angles of 93.1°. Experimental and computational studies of $FeMes_2$(SciOPP) are consistent with an intermediate-spin iron(II) complex (S = 1). The ground state wave function of $FeMes_2$(SciOPP) is described by two occupied β MO Fe d orbitals mixed with significant mesityl π character, as well as three unoccupied β MO Fe d orbitals (Figure 3). Other FMOs demonstrate significant Benz π^* MO character with mixed phosphorus character, representing a π-interaction between the phosphorus p and Benz p orbitals. The Fe−P bonding character is further described by the σ-interaction from phosphorus p orbitals with d_{xy} (β329) and the π-interaction through the d_{xz} and d_{yz} orbitals (β321 and β325, respectively). The d_{xy} orbital is found to be highest in energy due to Fe-Mes σ^* character present, most clearly seen in the corresponding α MO (α327). Notably, the d_{z2} orbital is unoccupied in the β manifold for the distorted square-planar complex.

2.2. Spectroscopic Determination of In Situ Generated Iron Species. While mono- and bis-mesityl complexes of SciOPP can be independently synthesized, it is essential to evaluate the iron species formed in situ in reactions of $FeCl_2$(SciOPP) with MesMgBr. These studies include reactions with stoichiometric and excess MesMgBr as well as elucidation of the iron species present in solution during catalytic reaction with primary alkyl halides.

2.2.1. In Situ Reactions of $FeCl_2$(SciOPP) with MesMgBr. The reaction of 3 mM $^{57}FeCl_2$(SciOPP) in 1:1 THF:2-MeTHF with 1 equiv of MesMgBr at room temperature led to the rapid generation of a deep yellow solution, which was freeze-trapped for Mössbauer and MCD measurements 5 min after Grignard addition. The 80 K Mössbauer spectrum (Figure 4A) could be fit to a single major iron species with δ = 0.52 mm/s and ΔE_Q = 2.10 mm/s. The observed isomer shift is identical to that previously determined for as-prepared FeBrMes(SciOPP) (Table 1), while the ΔE_Q value is slightly increased (2.10 mm/s vs 1.92 mm/s for the solid). Notably, the reaction of $^{57}FeBr_2$(SciOPP) in solution with 1 equiv of MesMgBr contains a single major iron species with δ = 0.52 mm/s and ΔE_Q = 2.12 mm/s (see SI Figure S3A, ∼94% of iron), further demonstrating that the monomesitylated species in solution exhibit a structural distortion compared to the solid state. The 5 K, 7 T NIR MCD spectrum of the solution generated iron species from reaction with 1 equiv of MesMgBr (Figure 4E) is identical to that previously determined for as-prepared FeBrMes(SciOPP) with two low-energy d−d transitions at ∼6460 and 7460 cm^{-1}. This observation is consistent with synthetic studies where the reaction of $FeCl_2$(SciOPP) with 1 equiv of MesMgBr leads to FeXMes(SciOPP) (X = Br:Cl in an ∼4:1 ratio based on single crystal studies, see SI) with significant halide exchange. Combined, the NIR MCD and Mössbauer data definitively show that in solution the reaction of $^{57}FeCl_2$(SciOPP) with 1 equiv of MesMgBr generates exclusively a monomesitylated tetrahedral complex, which is assigned as FeBrMes(SciOPP).

The reaction of 3 mM $^{57}FeCl_2$(SciOPP) with 2 equiv of MesMgBr at room temperature led to the rapid formation of a dark orange-red solution which was freeze-trapped for Mössbauer and MCD measurements 5 min after Grignard addition. The 80 K Mössbauer spectrum of the in situ generated species (Figure 4B) contains a single major species (∼90% of all iron) with parameters (δ = 0.28 mm/s and ΔE_Q = 3.67 mm/s) nearly identical to those of as-prepared $FeMes_2$(SciOPP). Furthermore, the NIR MCD spectrum of the solution generated species (Figure 4F) is also consistent with the as-prepared solid. The small difference observed in the freeze-trapped solution Mössbauer and MCD spectra of $FeMes_2$(SciOPP) are indicative of a very slight distortion of the complex in solution combined with the small contributions from the minor species also present. These minor species are clearly evident from the Mössbauer data and correspond to FeBrMes(SciOPP) (∼3% of iron) and a new iron species with δ = 0.21 mm/s and ΔE_Q = 1.43 mm/s (∼7% of iron). No EPR active species were observed (see SI, Figure S4, t = 0).

Table 1. ^{57}Fe Mössbauer Parameters for Iron-SciOPP and Iron-Mesityl Complexes

complex	sample	isomer shift (δ)[c]	ΔE_Q[c]
$FeCl_2$(SciOPP)[a]	frozen solution[b]	0.94 mm/s	2.69 mm/s
$FeBr_2$(SciOPP)[a]	frozen solution	0.92 mm/s	2.95 mm/s
FeBrMes(SciOPP)	solid	0.52 mm/s	1.97 mm/s
FeBrMes(SciOPP)	frozen solution	0.52 mm/s	2.12 mm/s
FeClMes(SciOPP)[a]	solid	0.53 mm/s	1.87 mm/s
$FeMes_2$(SciOPP)	solid	0.29 mm/s	3.58 mm/s
$FeMes_2$(SciOPP)	frozen solution	0.28 mm/s	3.67 mm/s
$FeMes_3^-$	solid	0.20 mm/s	1.44 mm/s
$FeMes_3^-$	frozen solution	0.21 mm/s	1.43 mm/s

[a]Mössbauer spectra are given in the SI. [b]All frozen solution samples prepared with ^{57}Fe enriched complex at 3 mM in 1:1 THF:2-MeTHF. [c]Mössbauer fitting errors are ±0.02 mm/s for δ and ±2% for ΔE_Q.

Scheme 3. In Situ Iron Speciation from Reaction of $FeCl_2$(SciOPP) with MesMgBr

$$FeCl_2L + MesMgBr \xrightarrow{RT} FeBrMesL + FeMes_2L + FeMes_3^-$$

1.00 (x equiv)

L = SciOPP	x =	FeBrMesL	$FeMes_2L$	$FeMes_3^-$
	1 equiv	1.00	0	0
	2 equiv	0.03(3)	0.90(3)	0.07(3)
	20 equiv	0	0.38(3)	0.62(3)
	100 equiv	0	0.02(3)	0.98(3)

dx.doi.org/10.1021/ja503596m | J. Am. Chem. Soc. 2014, 136, 9132−9143

The reaction of $^{57}FeCl_2$(SciOPP) with excess MesMgBr (20 equiv) results in the rapid formation of an orange solution which was freeze-trapped for Mössbauer and MCD measurements 5 min after Grignard addition. The 80 K Mössbauer spectrum of the in situ generated species (Figure 4C) contains two major iron complexes: $FeMes_2$(SciOPP) (~38% of iron) and the new iron species observed in the 2 equiv reaction (δ = 0.21 mm/s, ΔE_Q = 1.43 mm/s, ~62% of iron). The NIR MCD spectrum of the in situ generated iron species (Figure 4G) displays transitions due to the $FeMes_2$(SciOPP) species (i.e., the positive band at 9300 cm^{-1} and the negative tail at ~16 000 cm^{-1}) as well as two new, intense negative transitions centered around ~8200 cm^{-1}. In addition, the UV−vis MCD spectrum clearly shows both CT bands of the bis-mesityl complex as well as a new, intense band at 29 100 cm^{-1} (see SI, Figure S5). Thus, while the addition of excess MesMgBr results in the further formation of the δ = 0.21 mm/s species with new LF and CT MCD features, more than one-third of all the iron remains $FeMes_2$(SciOPP). No significant change in this distribution is observed over the course of 1h at RT (see SI, Figure S6).

The addition of 100 equiv of MesMgBr to $^{57}FeCl_2$(SciOPP) results in a colorless solution, where Mössbauer spectroscopy (Figure 4D) indicates that the δ = 0.21 mm/s species is predominant in solution (~98% of all iron in solution) with only a very minor amount of $FeMes_2$(SciOPP) remaining (~2%). On the basis of previous studies by Bedford and Fürstner with iron-catalyzed cross-couplings of MesMgBr, it was hypothesized that this new iron species might be the iron-ate species $[Mg_2X_3(THF)_6][FeMes_3]$ (denoted as $FeMes_3^-$).[31,35] To evaluate this possibility, ^{31}P and paramagnetic ^1H NMR studies of the 100 equiv of MesMgBr reaction sample were performed. The paramagnetic ^1H NMR spectrum of the iron species formed in situ with 100 equiv of MesMgBr are identical to those previously reported for $FeMes_3^-$ (see SI). Furthermore, the ^{31}P NMR spectrum of the 100 equiv reaction demonstrated the formation of free SciOPP ligand as expected upon the formation of $FeMes_3^-$ (see SI). Unambiguous confirmation of the formation of $FeMes_3^-$ was determined via Mössbauer and NIR MCD studies of independently synthesized $FeMes_3^-$. The 80 K Mössbauer spectrum of solid $FeMes_3^-$ is well-fit as a single iron species with δ = 0.20 mm/s and ΔE_Q = 1.44 mm/s (Figure 4I), nearly identical to the parameters for solution generated $FeMes_3^-$ from the reaction of $^{57}FeCl_2$·1.5THF with 3 equiv of MesMgBr (Figure 4J, δ = 0.21 mm/s and ΔE_Q = 1.43 mm/s). The solution $FeMes_3^-$ Mössbauer parameters are identical to the iron species formed in the presence of excess MesMgBr. The 5 K, 7 T NIR MCD (Figure 4H) of $FeMes_3^-$ from the 100 equiv of MesMgBr reaction displays two low energy LF bands at ~7340 and 8590 cm^{-1}. By comparison, the 5 K, 7 T NIR MCD (Figure 4K) of as-prepared $FeMes_3^-$ in 1:1 THF:2-MeTHF is essentially identical to that observed in the 100 equiv of MesMgBr reaction, with two low energy LF bands at ~7340 and 8590 cm^{-1}. Combined, these spectroscopic experiments definitively demonstrate that $FeMes_3^-$ is the additional iron species formed in the presence of excess MesMgBr. Reaction of $^{57}FeBr_2$(SciOPP) with MesMgBr also generates mixtures of $FeMes_2$(SciOPP) and $FeMes_3^-$ in the presence of excess MesMgBr (SI, Figure S3).

Lastly, the persistence of $FeMes_2$(SciOPP) even in the presence of a large excess of MesMgBr led to the hypothesis that SciOPP may be able to coordinate to $FeMes_3^-$. To test this, 2 equiv of SciOPP ligand was added to a 3 mM solution of in situ generated $FeMes_3^-$ (Figure 5). Prior to SciOPP addition, a Mössbauer spectrum identical to that reported for in situ generated $FeMes_3^-$ (Figure 4J) was obtained. The addition of SciOPP led to an immediate color change of the solution from colorless to dark red. The 80 K Mössbauer spectrum of the frozen solution following SciOPP addition indicated the formation of a mixture of $FeMes_2$(SciOPP) and $FeMes_3^-$, 80 and 20% of all iron in solution, respectively. ^1H NMR studies indicate that MesMgBr is also formed upon SciOPP addition (see SI). Therefore, SciOPP can ligate directly to $FeMes_3^-$ to lead to the generation of $FeMes_2$(SciOPP) and MesMgBr in solution.

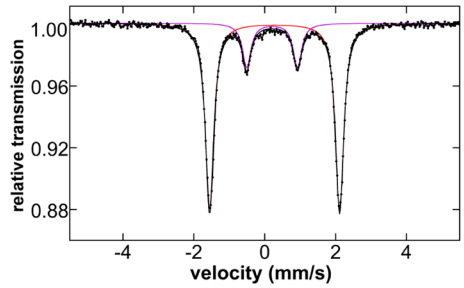

Figure 5. 80 K ^{57}Fe Mössbauer spectrum of the iron species formed in solution from the addition of 2 equiv of SciOPP ligand to in situ generated 3 mM $FeMes_3^-$ in 1:1 THF:2-MeTHF. Data (black dots), total fit (black line) and individual components are shown.

2.2.2. Iron Species Present In Situ During Catalytic Reaction. While the iron species formed in solution from reactions of $FeCl_2$(SciOPP) with MesMgBr have been elucidated, it is also important to directly evaluate the iron species formed in situ during catalysis to determine if additional iron species are generated in the presence of electrophile. To evaluate the iron species present during catalysis, the reported Kumada catalytic reaction for cross-coupling MesMgBr and 1-iododecane with $FeCl_2$(SciOPP) was performed at 40 °C using the slow addition method of MesMgBr previously reported,[18] but utilizing ^{57}Fe labeled precatalyst. A reaction sample was freeze-trapped at 25 min into the 3 h reaction and evaluated by Mössbauer spectroscopy. At this time point, a total of ~5.5 equiv of MesMgBr with respect to iron had been added. The 80 K Mössbauer spectrum of the 25 min reaction sample (Figure 6) is well-fit to two iron species, FeXMes(SciOPP) (δ = 0.51 mm/s, ΔE_Q = 2.16 mm/s) and $FeMes_2$(SciOPP) (δ = 0.28

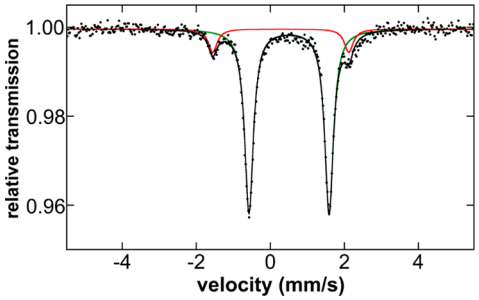

Figure 6. 80 K ^{57}Fe Mössbauer spectrum of the iron species present during the Kumada cross-coupling of MesMgBr and 1-iododecane by $^{57}FeCl_2$(SciOPP). The freeze-trapped sample was prepared 25 min into the 3 h catalytic reaction. Data (black dots), total fit (black line) and individual components are shown.

dx.doi.org/10.1021/ja503596m | J. Am. Chem. Soc. 2014, 136, 9132−9143

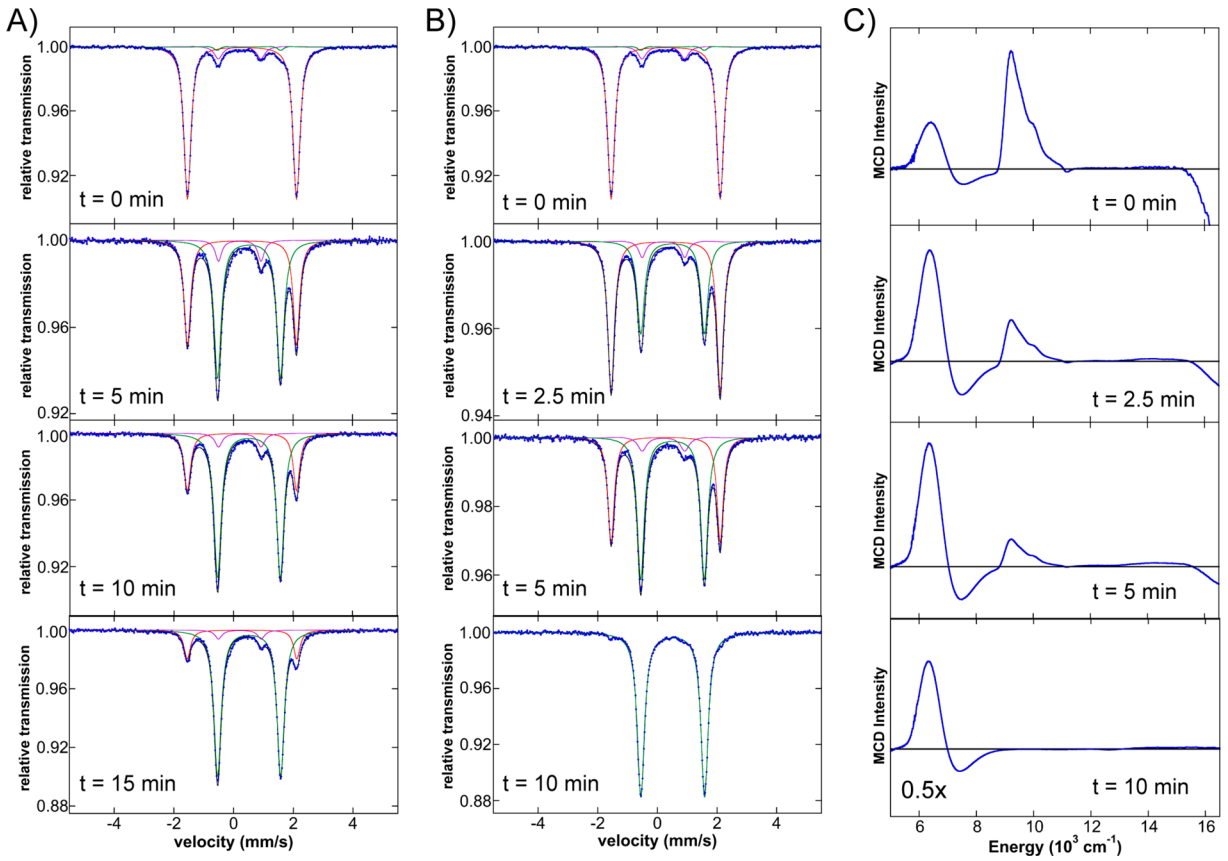

Figure 7. ^{57}Fe Mössbauer and MCD spectroscopy of the iron species present in situ in reactions of solution generated $FeMes_2$(SciOPP) with primary alkyl halides. 80 K ^{57}Fe Mössbauer spectrum of in situ generated $FeMes_2$(SciOPP)$_2$ in 1:1 THF:2-MeTHF and the spectra of freeze-trapped samples as a function of time following reaction with (A) 20 equiv of 1-bromodecane and (B) 20 equiv of 1-iododecane. Data (black dots) and total fits (black lines) are shown for each spectrum. Details of the individual components are given in the SI. (C) The 5 K, 7 T NIR MCD spectrum of in situ generated $FeMes_2$(SciOPP)$_2$ in 1:1 THF:2-MeTHF and the spectra of freeze-trapped samples as a function of time following reaction with 1-iododecane. All MCD spectra are shown with the same *y*-axis scale for direct comparison (the 10 min spectrum is shown at half-intensity to fit on the same scale).

mm/s, ΔE_Q = 3.67 mm/s) present at ~88 and ~12% of the iron in solution, respectively.

2.3. In Situ Spectroscopic Characterization of Reactions of $FeMes_2$(SciOPP) and $FeMes_3^-$ with Primary Alkyl Halide. *2.3.1. $FeMes_2$(SciOPP).* The in situ generated iron species from reaction of $FeCl_2$(SciOPP) with 2 equiv of MesMgBr were selected for these studies as they permitted the direct evaluation of the reactivity of in situ generated $FeMes_2$(SciOPP). Using ^{57}Fe labeled precatalyst and preparing freeze-trapped Mössbauer samples at well-defined time points, the reaction of in situ generated $FeMes_2$(SciOPP) (3 mM, from 2 equiv of MesMgBr reaction) with excess 1-bromodecane (20 equiv) at room temperature in 1:1 THF:2-MeTHF was investigated over the course of 15 min (Figure 7A). After 5 min of reaction time, the Mössbauer spectrum indicates the consumption of the square-planar $FeMes_2$(SciOPP) (red, ~90% at t = 0 to ~56% at t = 2.5 min, error ±3%) with the simultaneous generation of a new iron species with δ = 0.52 mm/s and ΔE_Q = 2.13 mm/s (green, ~37% of all iron at t = 2.5 min), consistent with the formation of FeBrMes(SciOPP) from our previous spectroscopic studies (vide supra). After 10 min of reaction, the bis(mesityl) species has reduced to ~24% of all iron while FeBrMes(SciOPP) continues to increase to ~69%. By 20 min of total reaction time, nearly all the $FeMes_2$(SciOPP) in solution has been consumed with near complete conversion to the monomesitylated species (see SI, Figure S7 for t = 20 min spectrum). Analogous reaction studies with 1-iododecane (Figure 7B) yield the same general reaction trend for the in situ iron species: consumption of $FeMes_2$(SciOPP) with the generation of FeXMes(SciOPP). By 10 min, only the FeXMes(SciOPP) species is present in solution.

Importantly, GC studies of the reaction of $FeMes_2$(SciOPP) (3 mM) with 1-iododecane (5 equiv) in 1:1 THF:2-MeTHF at RT indicate the formation of mesityldecane (77% yield with respect to iron after 30 min, 97% yield after 2 h with no detectable decane or decene formed at either time point, see SI). Similar results have recently been reported for the stoichiometric reaction of $FeMes_2$(SciOPP) with 1-iodoundecane (1.2 equiv) where 77% yield of mesitylundecane was obtained after reaction for 2.5 h at 70 °C.[31] In addition, no consumption of the FeXMes(SciOPP) species is observed spectroscopically over the reaction times investigated in the presence of excess electrophile, indicating their very limited reactivity compared to $FeMes_2$(SciOPP). This is confirmed by GC studies of the reaction of FeBrMes(SciOPP) (3 mM) with 1-bromodecane (5 equiv) where almost no reactivity was observed (<1% yield with respect to iron after 30 min and ~2% yield after 3 h, with <1% yield of decane and no detectable decene at either time point). By contrast to the highly selective formation of mesityldecane with $FeMes_2$(SciOPP), reaction of primary alkyl halide with $FeMes_3^-$ resulted in the formation of

dx.doi.org/10.1021/ja503596m | J. Am. Chem. Soc. 2014, 136, 9132−9143

nearly equal amounts of mesityldecane and decene (see SI), consistent with the poor selectivities reported for reaction of $FeMes_3^-$ with 1-bromooctane.[35]

The NIR MCD spectra of the reaction with 1-iododecane (Figure 7C) provide further evidence for this time-dependent conversion of $FeMes_2$(SciOPP) to FeXMes(SciOPP). This is most clearly shown by the loss of the LF bands of $FeMes_2$(SciOPP) (for example, the band at 9300 cm^{-1}) as a function of time with the simultaneous generation of new, intense LF bands at low energy. After 10 min of reaction, only two LF bands are present at 6350 and 7390 cm^{-1} ($10Dq(T_d) \sim 6870$ cm^{-1}), consistent with the formation of a single high-spin iron(II) tetrahedral species with features nearly identical to those previously observed for FeBrMes(SciOPP) complexes. The previously determined $10Dq(T_d)$ value for FeBrMes(SciOPP) (6960 cm^{-1}) is slightly larger than that observed for the in situ reaction generated tetrahedral iron complex, consistent with differences in the coordinated halide (Br vs I). Thus, Mössbauer and NIR MCD allow for the identification of the distorted tetrahedral species generated in solution upon reaction of distorted square-planar $FeMes_2$(SciOPP) with 1-iododecane as FeIMes(SciOPP).

Scheme 4. Reaction of $FeMes_2$(SciOPP) with Primary Alkyl Halides Determined by In Situ Mössbauer and GC Studies

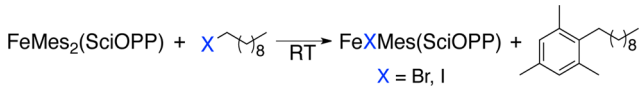

2.3.2. Kinetics of the Reaction of $FeMes_2$(SciOPP) and $FeMes_3^-$ with 1-Bromodecane. While $FeMes_2$(SciOPP) has been demonstrated herein to be competent in stoichiometric reactions with 1-bromodecane to yield mesityldecane, previous studies have shown that $FeMes_3^-$ can also undergo an analogous reaction to generate mesityldecane.[31,35] Since both $FeMes_2$(SciOPP) and $FeMes_3^-$ are formed in situ in reaction with excess MesMgBr (20 equiv), the relative rates of reaction of these two iron species (3 mM in 1:1 THF:2-MeTHF) with 1-bromodecane were investigated under pseudo-first-order conditions in the presence of excess electrophile (20 equiv). This kinetic information is obtainable via the previously described in situ, freeze-trapped reactions of $FeMes_2$(SciOPP) with 20 equiv of 1-bromodecane investigated by Mössbauer spectroscopy (section 2.3.1). Following the amount of $FeMes_2$(SciOPP) species present in solution as a function of reaction time, an observed rate constant of $2.4(3) \times 10^{-3}$ s^{-1} can be determined via a first-order kinetic fit (Figure 8).

Utilizing the same experimental approach, the reaction of in situ generated $FeMes_3^-$ (3 mM, from the reaction of $^{57}FeCl_2$ with 3 equiv of MesMgBr) with 20 equiv of 1-bromodecane at RT was investigated (see SI, Figure S8). This reaction was more complicated than that observed for $FeMes_2$(SciOPP) as the iron product further evolves over time in solution to generate a complex iron mixture. Nevertheless, the amount of $FeMes_3^-$ species present in solution as a function of reaction time could be determined and an observed rate constant of $1.7(3) \times 10^{-3}$ s^{-1} obtained via a first-order kinetic fit (Figure 8) for the rate of $FeMes_3^-$ consumption. Thus, initial reaction of $FeMes_3^-$ with 1-bromodecane occurs at a very similar rate as the reaction with $FeMes_2$(SciOPP) and, hence, significant differences in the rates of reaction of these two species would not be sufficient to result in exclusive reaction with

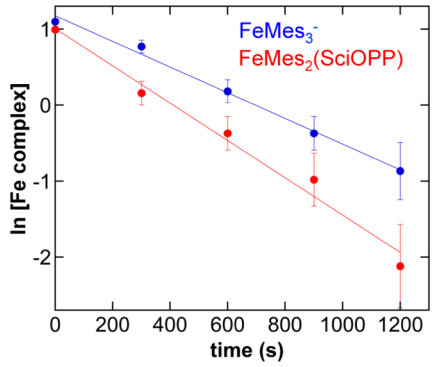

Figure 8. Pseudo-first-order kinetic data for reactions of in situ generated $FeMes_2$(SciOPP) and $FeMes_3^-$ with 20 equiv of 1-bromodecane using freeze-trapped ^{57}Fe Mössbauer spectroscopy.

$FeMes_2$(SciOPP) if a mixture is present. Lastly, it is interesting to note that the rapid evolution of the iron species in the $FeMes_3^-$ reaction with electrophile in solution over the time course investigated is consistent with our GC studies (see SI) and previous studies of the reaction of $FeMes_3^-$ with 1-bromoctane where multiple equivalents of electrophile are observed to react per iron, leading to nearly equal amounts of cross-coupled produced and β-hydrogen eliminated side product.[35] The reaction of the product iron species may occur more rapidly compared to initial $FeMes_3^-$ consumption and is a likely origin of the significant production of undesired side product observed with $FeMes_3^-$.

3. DISCUSSION

The elucidation of in situ iron speciation, active catalyst structure and the mechanism of iron-catalyzed C−C cross-coupling has remained a significant challenge through traditional characterization methods due to many of the unique challenges present in these systems, including the potential for complex mixtures of paramagnetic species. In the present study, an experimental methodology combining ^{57}Fe Mössbauer, MCD and DFT investigations combined with inorganic synthesis of well-defined mesitylated iron(II) species has been demonstrated to provide unprecedented insight into the Kumada catalyzed cross-coupling of MesMgBr and primary alkyl halides. Importantly, this experimental methodology directly addresses many of the challenges present in studying iron-based cross coupling systems including: (1) elucidation and quantification of mixtures of in situ formed paramagnetic iron(II)-SciOPP species using freeze-trapped solution Mössbauer, (2) detailed electronic structure and bonding in iron(II)-SciOPP species using MCD spectroscopy and DFT calculations and (3) direct investigation of the reaction of in situ formed mesityl-iron(II) species with primary alkyl halides by Mössbauer and MCD spectroscopies.

In terms of in situ iron speciation, three different mesitylated iron(II) species can be formed in situ in reactions of the $FeCl_2$(SciOPP) precatalyst with MesMgBr. At low equivalents of MesMgBr, FeBrMes(SciOPP) (at 1 equiv) and $FeMes_2$(SciOPP) (2 equiv) dominate in solution, whereas the addition of excess MesMgBr leads to the formation of $FeMes_3^-$ with loss of the SciOPP ligand. However, the addition of free SciOPP ligand to $FeMes_3^-$ leads to the formation of a mixture of $FeMes_2$(SciOPP) and $FeMes_3^-$. Combined with the incomplete formation of $FeMes_3^-$ even in the presence of a large excess of MesMgBr, these studies demonstrate that a

dx.doi.org/10.1021/ja503596m | J. Am. Chem. Soc. 2014, 136, 9132−9143

mixture of $FeMes_2$(SciOPP) and $FeMes_3^-$ exists in solution, where the amount of each species is dependent on the amount of MesMgBr and SciOPP present. In addition, direct evaluation of the iron species present during catalysis with 1-iododecane indicate the presence of FeXMes(SciOPP) and $FeMes_2$(SciOPP). The absence of detectable $FeMes_3^-$ during catalysis results from the slow rate of addition of MesMgBr employed in the catalytic reaction, thus limiting the amount of excess MesMgBr present in solution at any point in time.

Spectroscopic studies of the reaction of in situ generated $FeMes_2$(SciOPP) in combination with GC studies establish that $FeMes_2$(SciOPP) is the active species involved in the Kumada cross-coupling of MesMgBr and primary alkyl halides. The reaction protocol employed for catalysis involves both slow MesMgBr addition as well as free SciOPP ligand as a reaction additive, both of which serve to minimize the formation of $FeMes_3^-$ and maximize the selective formation of active $FeMes_2$(SciOPP) during catalysis. This effect is critical for high product selectivity for mesityldecane, as our GC studies and previous stoichiometric studies of the reaction of $FeMes_3^-$ with primary alkyl halides indicate the formation of significant decene side product.[31,35] Since reactions of $FeMes_3^-$ and $FeMes_2$(SciOPP) with electrophile occur at similar rates but give very different selectivities, the suppression of the formation of $FeMes_3^-$ through SciOPP ligation and the slow addition protocol are essential for obtaining highly selective formation of cross-coupled product. While the slow addition method also leads to the presence of a large amount of FeXMes(SciOPP) in solution, the in situ reaction studies monitored by Mössbauer spectroscopy and GC studies clearly demonstrate that FeXMes(SciOPP) species exhibit minimal reactivity compared to $FeMes_2$(SciOPP). This is demonstrated by (1) the lack of FeXMes(SciOPP) consumption during the reaction time (10–20 min depending on the primary alkyl halide) required for complete consumption of $FeMes_2$(SciOPP) and (2) the minimal reactivity observed by GC in reactions of FeBrMes(SciOPP) with 1-bromodecane.

In situ Mössbauer and MCD studies of the reaction of $FeMes_2$(SciOPP) with primary alkyl halides also provide direct insight into the mechanism of catalysis operating in these systems. A previous mechanistic proposal for C–C cross-coupling catalysis by $FeCl_2$(SciOPP) with aryl nucleophiles involves an Fe^{II}/Fe^{III} redox cycle (Scheme 5) with direct reaction of Fe(aryl)$_2$(SciOPP) with electrophile (R–X) to generate product and Fe(aryl)(X)(SciOPP) (via an Fe^{III}(aryl)$_2$(X)/R$^\bullet$ intermediate).[17,18] Our in situ reaction studies of the pseudo- first order reactions of $FeMes_2$(SciOPP) with primary alkyl halides demonstrate that the reaction of $FeMes_2$(SciOPP) with electrophile leads to the clean formation of the corresponding FeXMes(SciOPP) species (X = Br, I). In contrast to previous proposals for iron-bisphosphine cross-coupling systems utilizing dpbz and dppe ligands,[20,24] EPR studies indicate no observed formation of iron(I) species (S = 1/2 or S = 3/2) (see Figure S4, SI). Our spectroscopic studies following the iron species formed in situ upon the reaction of $FeCl_2$(SciOPP) with MesMgBr also clearly show that while the addition of 1 equiv of MesMgBr leads to the formation of FeBrMes(SciOPP), a second equivalent of MesMgBr leads to the predominant formation of $FeMes_2$(SciOPP). These observations are in direct accordance with the previous mechanistic proposal, where the intermediate iron(III) species is expected to be very short-lived and would be unlikely to accumulate to a detectable level during catalysis—consistent with no Mössbauer signals corresponding to generation of this species. Previous radical clock studies of the Kumada cross-coupling of MesMgBr and iodomethylcyclopropane would be consistent with such an iron(III)–X intermediate and R$^\bullet$ with rapid recombination,[18] perhaps via a radical rebound mechanism. We consider an iron(IV) intermediate to be an unlikely pathway due to both the radical clock experiments and the bisphosphine ligation, where the oxidation of the iron-bisphosphine species to iron(IV) would be unfavorable.

Upon the basis of this mechanism, further insight into the high reactivity of $FeMes_2$(SciOPP) compared to FeBrMes(SciOPP) can be derived from the unique electronic structure and geometry of $FeMes_2$(SciOPP). For catalysis, an unoccupied and low-lying FMO with significant metal character and proper orientation for overlap with substrate is required. From our DFT studies of $FeMes_2$(SciOPP), the unoccupied d_{z2} orbital (β326, Figure 3) is low-lying and oriented in a sterically accessible direction in the distorted square planar structure for good overlap and σ-interaction with the electrophile for homolytic bond cleavage. Importantly, the distortion from pure square planar geometry of $FeMes_2$(SciOPP) ensures that d_{z2} is unoccupied as this distortion results in a slight increase in energy of d_{z2}. While the d_{yz} and d_{xy} orbitals (β325 and β329, respectively) are also unoccupied, these are less accessible for substrate activation due to the steric bulk of the SciOPP and mesityl ligands. By contrast, the tetrahedral geometry of FeBrMes(SciOPP) results in sterically inaccessible unoccupied d orbitals. The unoccupied d_{z2} orbital is obstructed by the bromine atom and mesityl ligand (β309, Figure 2) while the orientations of the $d_{xz/yz}$ orbitals are also unfavorable for substrate activation. Therefore, reaction of FeBrMes(SciOPP) with electrophile would require a significant distortion of the tetrahedral structure for substrate activation which would be energetically unfavorable.

The iron-SciOPP catalyzed cross-coupling of MesMgBr and primary alkyl halides investigated herein also provides an interesting contrast to iron-TMEDA chemistry. Bedford and co-workers have demonstrated that the reaction of $FeCl_2$ with even small excesses of MesMgBr (4 equiv) leads to the exclusive formation of $FeMes_3^-$ and it was proposed that such a iron-ate species may predominate in catalysis with TMEDA.[35] This proposal is further supported by reaction studies that demonstrate that $FeMes_3^-$ reacts much more rapidly with 1-

Scheme 5. Proposed Mechanism by Nakamura for $FeCl_2$(SciOPP) Catalyzed Cross-Coupling of Aryl Nucleophiles and Alkyl Electrophiles[17,18]

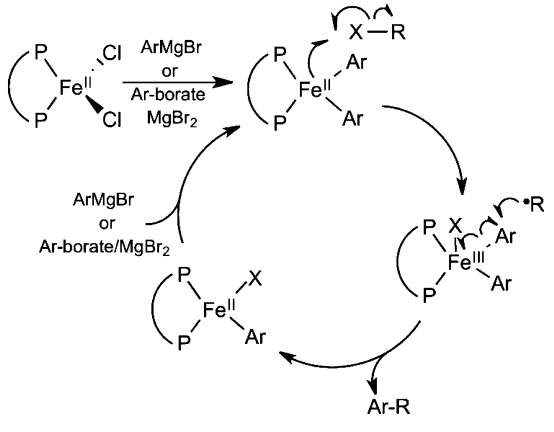

dx.doi.org/10.1021/ja503596m | J. Am. Chem. Soc. 2014, 136, 9132–9143

bromooctane to generate mesityloctane than does $FeMes_2$(TMEDA). By contrast, $FeCl_2$(SciOPP) is a highly selective precatalyst for cross-coupled product. This selectivity derives from the fact that catalysis in iron-SciOPP proceeds via $FeMes_2$(SciOPP) due to the presence of this species in solution even in large excess of MesMgBr. Combined with the slow addition of nucleophile and excess SciOPP ligand added in the catalytic reaction (which has been shown herein to convert $FeMes_3^-$ to $FeMes_2$(SciOPP)), improved activity and selectivity in iron-SciOPP catalysis occurs relative to iron-TMEDA catalyzed cross-coupling of MesMgBr and primary alkyl halides.

Finally, while the elucidation of the in situ formed iron species in $FeCl_2$(SciOPP) cross-coupling with MesMgBr represents a significant advance in our understanding of iron-bisphosphine cross-coupling, care should be taken not to generalize the observed species and mechanism to other iron-bisphosphine catalyzed reactions. The mesityl ligand is unique as the resulting bis-mesityl species is stable toward reductive elimination. This is unlikely to be true for other aryl nucleophiles (e.g., phenyl) and, hence, the iron species and reaction pathways may be more complex. Beyond nucleophile effects, we also expect the nature of the bisphosphine ligand to have a significant effect on in situ iron reduction pathways and speciation. Thus, each unique system requires a detailed in situ investigation in order to establish the variety of iron species and cross-coupling mechanisms that may be present in iron-bisphosphine cross-coupling catalysis. Importantly, the general research methodology described herein is amenable to application across the breadth of iron cross-coupling systems, where the ability to freeze-trap iron intermediates will facilitate the investigation of very rapid iron transformations in cross-coupling.

4. CONCLUSION

In the present study, a combination of Mössbauer, MCD and DFT methods has been demonstrated to be a highly impactful methodology for the investigation of iron-catalyzed Kumada coupling of MesMgBr and primary alkyl halides. These studies permit the identification of $FeMes_2$(SciOPP) as the active catalyst, and detailed MCD and DFT/TD-DFT studies provide detailed insight into electronic structure and bonding in this species. In addition, in situ studies of the reaction of $FeMes_2$(SciOPP) with primary alkyl halides using freeze-trapped Mössbauer and MCD spectroscopies is shown to generate FeXMes(SciOPP) (X = halide) along with the formation of mesityldecane, consistent with previous proposals of an iron(II)/iron(III) catalytic mechanism. The further application of this combined spectroscopic, synthetic and theoretical approach to additional iron C−C cross-coupling systems should continue to unravel the key iron species and mechanisms active in this catalysis.

5. EXPERIMENTAL SECTION

5.1. General Considerations. All reagents were purchased from commercial sources. All air and moisture sensitive manipulations were carried out in an MBraun inert-atmosphere (N_2) drybox equipped with a direct liquid nitrogen inlet line. All anhydrous solvents were further dried using activated alumina/4 Å molecular sieves and stored under inert-atmosphere over molecular sieves. $^{57}FeCl_2$(SciOPP) and $^{57}FeBr_2$(SciOPP) were prepared following literature methods[17] from $^{57}FeCl_2$·1.5THF and $^{57}FeBr_2$, respectively. $^{57}FeCl_2$·1.5THF and $^{57}FeBr_2$ were synthesized following literature procedures[36] using ^{57}Fe metal (95% enriched) purchased from Isoflex. $FeMes_3^-$ was prepared following published literature methods.[37]

5.2. Synthesis of $FeMes_2$(SciOPP) and FeBrMes(SciOPP). *$Fe(Mes)_2$SciOPP.* To a stirring solution of $FeCl_2$(SciOPP) (100 mg, 0.098 mmol) in THF (10 mL) at −30 °C was added 2.2 equiv of mesitylmagnesium bromide (215 μL of a 1.0 M solution in THF) dropwise. The addition of Grignard reagent produced at first a yellow solution, which became deep red-orange as the addition progressed. The solution was filtered through a pad of Celite before all volatiles were removed in vacuo. The residue was extracted with a 1:1 ether/pentane solution and filtered. After drying, single crystals suitable for X-ray diffraction were obtained from slow evaporation of a toluene/pentane solution. Bulk crystals could be grown from storage of the mother liquor at −30 °C (114 mg collected, 98% yield). ^1H NMR (500 MHz, C_6D_6) δ 78.7, 72.0, 61.7, 12.1. Anal. Calcd for $C_{80}H_{110}P_2Fe$: 80.77 C, 9.32 H. Found: 80.93 C, 9.94 H. μ_{eff} (C_6D_6) = 4.1(3) μ_B.

FeBrMes(SciOPP). To a stirring solution of $FeBr_2$(SciOPP) (86 mg, 0.077 mmol) in THF (10 mL) was added 1.0 equiv of mesitylmagnesium bromide (76 μL of a 1.0 M solution in THF) dropwise resulting in a color change from pale brown to yellow. The solution was filtered through a pad of Celite before all volatiles were removed in vacuo. The residue was then extracted with a 1:1 ether/pentane mixture and filtered. The filtrate was concentrated to ∼2 mL and stored at −30 °C resulting in the formation of yellow crystals (57 mg collected, 64% yield). ^1H NMR (500 MHz, C_6D_6) δ 152.8, 121.4, 86.9, 28.4, 10.0, −7.5, −10.0. Calcd for $C_{71}H_{99}P_2FeBr$ with one molecule of diethyl ether ($C_4H_{10}O$): 73.57 C, 8.97 H. Found: 72.73 C, 8.51 H. μ_{eff} (C_6D_6) = 5.0(3) μ_B.

5.3. Mössbauer Spectroscopy. All solid samples for ^{57}Fe Mössbauer spectroscopy were run on nonenriched samples of the as-isolated complexes. Solution samples for ^{57}Fe Mössbauer spectroscopy were prepared from 3 mM $^{57}FeCl_2$(SciOPP) or $^{57}FeBr_2$(SciOPP) in 1:1 (v:v) THF:2-MeTHF to enable the simultaneous preparation of Mössbauer and MCD samples. All samples were prepared in an inert atmosphere glovebox equipped with a liquid nitrogen fill port to enable sample freezing to 77 K within the glovebox. Each sample was loaded into a Delrin Mössbauer sample cup for measurements and loaded under liquid nitrogen. Low temperature ^{57}Fe Mössbauer measurements were performed using a See Co. MS4 Mössbauer spectrometer integrated with a Janis SVT-400T He/N_2 cryostat for measurements at 80 K with a 0.07 T applied magnetic field. Isomer shifts were determined relative to α-Fe at 298 K. All Mössbauer spectra were fit using the program WMoss (SeeCo).

5.4. Magnetic Circular Dichroism Spectroscopy. All samples for MCD spectroscopy were prepared in an inert atmosphere glovebox equipped with a liquid nitrogen fill port to enable sample freezing to 77 K within the glovebox. MCD samples were prepared in 1:1 (v:v) THF:2-MeTHF (to form low temperature optical glasses) in copper cells fitted with quartz disks and a 2 mm gasket. Low temperature MCD experiments were conducted using two Jasco spectropolarimeters. Both instruments utilize a modified sample compartment incorporating focusing optics and an Oxford Instruments SM4000−7T superconducting magnet/cryostat. This setup permits measurements from 1.6 to 290 K with magnetic fields up to 7 T. A calibrated Cernox sensor directly inserted in the copper sample holder is used to measure the temperature at the sample to 0.001 K. UV−visible MCD spectra were collected using a Jasco J-715 spectropolarimeter and a shielded S-20 photomultiplier tube. Near-infrared (NIR) data were collected with a Jasco J-730 spectropolarimeter and a liquid nitrogen cooled InSb detector. All MCD spectra were baseline-corrected against zero-field scans. VTVH-MCD spectra were analyzed using previously reported fitting procedures.[38,39]

5.5. Electronic Structure Calculations. Spin unrestricted density functional theory (DFT) calculations were performed with the Gaussian 09 package.[40] All geometry optimization calculations were performed with the PBEPBE[41] exchange-correlation functional with the TZVP[42] basis set on all atoms with the inclusion of solvation effects using the polarized continuum model (PCM) with tetrahydrofuran as the solvent.[43] The geometries of all complexes were fully

dx.doi.org/10.1021/ja503596m | J. Am. Chem. Soc. 2014, 136, 9132−9143

optimized starting from X-ray crystal structures with initial optimization performed with cep-4g before optimizing at the TZVP level. All optimized geometries had frequencies found to be real. Energies given include zero-point and thermal corrections.

Further calculations of MOs and time-dependent density function theory (TD-DFT) used the B3LYP functional with the TZVP basis set on all atoms. Molecular orbital (MO) compositions and analysis were calculated using the AOMix program.[44,45] Atomic charges and spin densities were calculated using Mulliken population analysis methods (MPA). Orbitals from the Gaussian calculations were plotted with the ChemCraft program. TD-DFT was used to calculate the electronic transition state energies and intensities of the 30−40 lowest-energy states. Simulated spectra were plotted with the Chemcraft program with half-widths of 2500 cm^{-1}.

5.6. Reactions of $FeMes_2$(SciOPP) and $FeMes_3^-$ with Electrophile for In Situ Spectroscopic Studies. As an example of the general procedure employed, the reaction of $^{57}FeMes_2$(SciOPP) with 20 equiv of 1-iododecane is described. To a 3 mM solution of $^{57}FeCl_2$(SciOPP) in a 1:1 THF:2-MeTHF solution was added dropwise 2.0 equiv of MesMgBr at RT to prepare $^{57}FeMes_2$(SciOPP) in solution. The solution was stirred for 5 min and Mössbauer and MCD samples were prepared and frozen in liquid nitrogen within an anaerobic glovebox. To the remaining solution was added 20 equiv of 1-iododecane. Samples for Mössbauer and MCD were simultaneously prepared at various time points (e.g., 2.5 min, 5 min, 10 min) and immediately frozen in liquid nitrogen to freeze trap the reaction at the desired time point.

5.7. Reaction of $FeMes_2$(SciOPP) with 1-Iododecane. To a solution of $FeMes_2$(SciOPP) (11.9 mg, 0.010 mmol) in 1:1 THF:2-MeTHF (3.3 mL) was added dodecane (8.5 mg, 0.050 mmol) and 1-iododecane (13.4 mg, 0.050 mmol) at room temperature. At 0.5, 1, 1.5, 2, 2.5, and 3 h time points the reaction mixture was quenched with 0.03:1 $Na_2SO_{4(aq)}$(1.0 M):THF and filtered through a pad of Florisil. Yields of mesityldecane and recovery of 1-iododecane were determined by quantitative GC analysis.

■ ASSOCIATED CONTENT

Ⓢ Supporting Information

Supplementary figures including Mössbauer, MCD, EPR, NMR and GC data; DFT optimized geometry coordinates; X-ray crystal structure data (CIF). This material is available free of charge via the Internet at http://pubs.acs.org.

■ AUTHOR INFORMATION

Corresponding Author

neidig@chem.rochester.edu

Author Contributions

†S. L. Daifuku and M. H. Al-Afyouni contributed equally.

Notes

The authors declare no competing financial interest.

■ ACKNOWLEDGMENTS

This work was supported by start-up funding from the University of Rochester. The authors thank Dr. William W. Brennessel for assistance in the collection and analysis of X-ray crystallographic data and Prof. Patrick L. Holland (Yale) for use of a syringe pump for catalytic studies. We also acknowledge the Center for Integrated Research Computing at the University of Rochester for providing the necessary computing systems and personnel to enable the research presented in this manuscript.

■ REFERENCES

(1) Bolm, C.; Legros, J.; Paih, J. L.; Zani, L. *Chem. Rev.* **2004**, *104*, 6217.

(2) Sherry, B. D.; Furstner, A. *Acc. Chem. Res.* **2008**, *41*, 1500.

(3) Czaplik, W. M.; Mayer, M.; Cvengros, J.; Wangelin, A. J. v. *ChemSusChem* **2009**, *2*, 396.

(4) Jana, R.; Pathak, T. P.; Sigman, M. S. *Chem. Rev.* **2011**, *111*, 1417.

(5) Tamura, M.; Kochi, J. K. *J. Am. Chem. Soc.* **1971**, *93*, 1487.

(6) Tamura, M.; Kochi, J. K. *J. Organomet. Chem.* **1971**, *31*, 289.

(7) Neumann, S. M.; Kochi, J. K. *J. Org. Chem.* **1975**, *40*, 599.

(8) Nakamura, M.; Matsuo, K.; Ito, S.; Nakamura, E. *J. Am. Chem. Soc.* **2004**, 3686.

(9) Guerinot, A.; Reymond, S.; Cossy, J. *Angew. Chem., Int. Ed.* **2007**, *46*, 6521.

(10) Cahiez, G.; Duplais, C.; Moyeaux, A. *Org. Lett.* **2007**, *9*, 3253.

(11) Noda, D.; Sunada, Y.; Hatakeyama, T.; Nakamura, M.; Nagashima, H. *J. Am. Chem. Soc.* **2009**, *131*, 6078.

(12) Bedford, R. B.; Betham, M.; Bruce, D. W.; Danopoulos, A. A.; Frost, R. M.; Hird, M. *J. Org. Chem.* **2006**, *71*, 1104.

(13) Ghorai, S.; Jin, M.; Hatakeyama, T.; Nakamura, M. *Org. Lett.* **2012**, *14*, 1066.

(14) Hatakeyama, T.; Nakamura, M. *J. Am. Chem. Soc.* **2007**, *129*, 9844.

(15) Hatakeyama, T.; Hashimoto, S.; Ishizuka, K.; Nakamura, M. *J. Am. Chem. Soc.* **2009**, *131*, 11949.

(16) Guisan-Ceinos, M.; Tato, F.; Bunuel, E.; Calle, P.; Cardenas, D. J. *Chem. Sci.* **2013**, *4*, 1098.

(17) Hatakeyama, T.; Hashimoto, T.; Kondo, Y.; Fujiwara, Y.; Seike, H.; Takaya, H.; Tamad, Y.; Ono, T.; Nakamura, M. *J. Am. Chem. Soc.* **2010**, *132*, 10674.

(18) Hatakeyama, T.; Fujiwara, Y.; Okada, Y.; Itoh, T.; Hashimoto, T.; Kawamura, S.; Ogata, K.; Takaya, H.; Nakamura, M. *Chem. Lett.* **2011**, *40*, 1030.

(19) Hatakeyama, T.; Okada, Y.; Yoshimoto, Y.; Nakamura, M. *Angew. Chem., Int. Ed.* **2011**, *50*, 10973.

(20) Adams, C. J.; Bedford, R. B.; Carter, E.; Gower, N. J.; Haddow, M. F.; Harvey, J. N.; Huwe, M.; Cartes, M. A.; Mansell, S. M.; Mendoza, C.; Murphy, D. M.; Neeve, E. C.; Nunn, J. *J. Am. Chem. Soc.* **2012**, *134*, 10333.

(21) Hatakeyama, T.; Kondo, Y.; Fujiwara, Y.; Takaya, H.; Ito, S.; Nakamura, E.; Nakamura, M. *Chem. Commun.* **2009**, 1216.

(22) Bedford, R. B.; Carter, E.; Cogswell, P. M.; Gower, N. J.; Haddow, M. F.; Harvey, J. N.; Murphy, D. M.; Neeve, E. C.; Nunn, J. *Angew. Chem., Int. Ed.* **2013**, *125*, 1323.

(23) Bedford, R. B.; Huwe, M.; Wilkinson, M. C. *Chem. Commun.* **2009**, 600.

(24) Bedford, R. B.; Carter, E.; Cogswell, P. M.; Gower, N. J.; Haddow, M. F.; Harvey, J. N.; Murphy, D. M.; Neeve, E. C.; Nunn, J. *Angew. Chem., Int. Ed.* **2013**, *52*, 1285.

(25) Hatakeyama, T.; Hashimoto, T.; Kathriarachchi, K. K. A. D. S.; Zenmyo, T.; Seike, H.; Nakamura, M. *Angew. Chem., Int. Ed.* **2012**, *51*, 8834.

(26) Dongol, K. G.; Koh, H.; Sau, M.; Chai, C. L. L. *Adv. Synth. Catal.* **2007**, *349*, 1015.

(27) Hashimoto, T.; Hatakeyama, T.; Nakamura, M. *J. Org. Chem.* **2011**, *77*, 1168.

(28) Kawamura, S.; Kawabata, T.; Ishizuka, K.; Nakamura, M. *Chem. Commun.* **2012**, *48*, 9376.

(29) Kawamura, S.; Ishizuka, K.; Takaya, H.; Nakamura, M. *Chem. Commun.* **2010**, *46*, 6054.

(30) Kawamura, S.; Nakamura, M. *Chem. Lett.* **2013**, *42*, 183.

(31) Sun, C.-L.; Krause, H.; Furstner, A. *Adv. Synth. Catal.* **2014**, *356*, 1281.

(32) Hawrelak, E. J.; Bernskoetter, W. H.; Lobkovsky, E.; Yee, G. T.; Bill, E.; Chirik, P. J. *Inorg. Chem.* **2005**, *44*, 3103.

(33) The VTVH-MCD data were best described using a -ZFS ground state model. The large magnitude of D is somewhat reduced compared to previous studies of a S = 1 square-planar iron(II) complex from magnetic susceptibility studies (Ray, K.; Begum, A.; Weyhermuller, T.; Piligkos, S.; Slageren, J. v.; Neese, F.; Wieghardt, K. *J. Am. Chem. Soc.* **2005**, *127*, 4403), consistent with the distorted square-planar structure of FeMes2(SciOPP).

(34) Geometry optimizations using the B3LYP functional gave poor agreement to X-ray crystallographic data with highly enlongated Fe−P bonds.
(35) Bedford, R. B.; Brenner, P. B.; Carter, E.; Cogswell, P. M.; Haddow, M. F.; Harvey, J. N.; Murphy, D. M.; Nunn, J.; Woodall, C. H. *Angew. Chem., Int. Ed.* **2014**, *53*, 1804.
(36) Winter, G.; Thompson, D. W.; Loehe, J. R. *Inorg. Synth.* **1973**, *14*, 99.
(37) Seidel, V. W.; Lattermann, K.-J. *Z. Anorg. Allg. Chem.* **1982**, *488*, 69.
(38) Pavel, E. G.; Kitajima, N.; Solomon, E. I. *J. Am. Chem. Soc.* **1998**, *120*, 3949.
(39) Neese, F.; Solomon, E. I. *Inorg. Chem.* **1999**, *38*, 1847.
(40) Frisch, M. J.; Trucks, G. W.; Schlegel, H. B.; Scuseria, G. E.; Robb, M. A.; Cheeseman, J. R.; Scalmani, G.; Barone, V.; Mennucci, B.; Petersson, G. A.; Nakatsuji, H.; Caricato, M.; Li, X.; Hratchian, H. P.; Izmaylov, A. F.; Bloino, J.; Zheng, G.; Sonnenberg, J. L.; Hada, M.; Ehara, M.; Toyota, K.; Fukuda, R.; Hasegawa, J.; Ishida, M.; Nakajima, T.; Honda, Y.; Kitao, O.; Nakai, H.; Vreven, T.; Montgomery, J. A., Jr.; Peralta, J. E.; Ogliaro, F.; Bearpark, M.; Heyd, J. J.; Brothers, E.; Kudin, K. N.; Staroverov, V. N.; Keith, T.; Kobayashi, R.; Normand, J.; Raghavachari, K.; Rendell, A.; Burant, J. C.; Iyengar, S. S.; Tomasi, J.; Cossi, M.; Rega, N.; Millam, J. M.; Klene, M.; Knox, J. E.; Cross, J. B.; Bakken, V.; Adamo, C.; Jaramillo, J.; Gomperts, R.; Stratmann, R. E.; Yazyev, O.; Austin, A. J.; Cammi, R.; Pomelli, C.; Ochterski, J. W.; Martin, R. L.; Morokuma, K.; Zakrzewski, V. G.; Voth, G. A.; Salvador, P.; Dannenberg, J. J.; Dapprich, S.; Daniels, A. D.; Farkas, Ö.; Foresman, J. B.; Ortiz, J. V.; Cioslowski, J.; Fox, D. J. *Gaussian 09*, Revision D.01; Gaussian, Inc.: Wallingford, CT, 2013.
(41) Perdew, J. P.; Burke, K.; Ernzerhof, M. *Phys. Rev. Lett.* **1996**, *77*, 3865.
(42) Schafer, A.; Huber, C.; Ahlrichs, R. *J. Chem. Phys.* **1994**, *100*, 5829.
(43) Tomasi, J.; Mennucci, B.; Cammi, R. *Chem. Rev.* **2005**, *105*, 2999.
(44) Gorelsky, S. I. *AO Mix: Program for Molcular Orbital Analysis*, http://www.sgchem.net/, version 6.8.5, 2014.
(45) Gorelsky, S. I. *J. Organomet. Chem.* **2001**, *635*, 187.